Article type: Communication

Dynamically Controlled Iridescence of Cholesteric Cellulose Nanocrystal Suspensions using Electric Fields

By *Bruno Frka-Petesic*, Harisoa Radavidson, Bruno Jean* and *Laurent Heux*

((Optional Dedication))

[*] Dr. B. Frka-Petesic, Dr. H. Radavidson, Dr. B. Jean, Dr. L. Heux
Centre de Recherche sur les Macromolecules Végétales (CERMAV-CNRS),
Université Grenoble Alpes, F-38000 Grenoble (France)
E-mail: bf284@cam.ac.uk

Keywords: cellulose nanocrystals, cholesteric, electric field, iridescence, colloidal liquid crystals

Online abstract:

Cellulose nanocrystal suspensions in apolar solvent spontaneously form iridescent liquid crystalline phases but the control of their long-range order is usually poor. We demonstrate how the use of electric fields can provide control on the cholesteric orientation and its local periodicity, allowing macroscopic sample homogeneity and dynamical tuning of their iridescent hues.

Many examples of photonic structures found in insects,[1-5] plants[6,7] or birds[8,9] still challenge our capabilities to fabricate equivalent man-made materials with controlled order from the nanoscale to the macroscale.[10-13] While the underlying biological processes enable a subtle balance of order and disorder to span over different lenghtscales, the precise design of biomimetic materials based on self-assembly strategies relies on the variety and the quality of our *toolbox* to drive the elementary building blocks toward the targeted structure. A successful control of the self-assembly routes is also key to allow a scalable and low cost production of novel nanostructured materials with enhanced optical properties.

Among eligible nanoparticles, cellulose nanocrystals (CNCs) provide a unique combination of features that offer a wide range of application prospects in high-added value functional

nanostructured materials.[13-17] These biosourced, lightweight and stiff nanorods, about 100-200 nm long and 5-15 nm in cross-section when extracted from cotton or woodpulp, indeed form stable colloidal suspensions and are able to spontaneously self-organize into cholesteric liquid crystalline phases above a threshold concentration.[18,19] This cholesteric structure is firstly attracting a strong interest as it is generally observed in natural cellulose- and chitin-based tissues of plants,[7] crabs[20,21] and insects,[3] where it provides either enhanced mechanical properties such as both stiffness and anti-crack propagation, or optical properties such as structural coloration and iridescence. Secondly, this property of CNCs has been exploited to generate thin solid films displaying adjustable colours[22-27] and also led to the development of active mesoporous cellulosic or inorganic photonic sensing materials constructed through nanotemplating strategies.[17,28-31] Moreover, the incorporation inside the cholesteric structure of anisometric dopants such as plasmonic gold nanorods provides additional control over their positional and orientational order inducing a chiroptical response templated by the CNC chiral assembly.[32-35]

However, a lack of satisfactory long-range ordering is often observed in these self-assembled structures. A polydomain structure with cracks, defects and misalignments between the domain is usually obtained, leading to pixelated and rainbow coloration rather than vivid optical effects.[36]

Increasing the long-range order of CNC cholesteric suspensions has been addressed by using different processes and triggers: while strong hydrodynamic shear disrupts the cholesteric order and turns it into a nematic one[37,38], Lagerwall and co-workers[39,40] reported how mild circular shear applied to a drying suspension in a circular dish leads to a locally enhanced vertical cholesteric orientation. However, in the latter case, a gradual distorsion of the helicoidal ordering towards the edge was obtained. Using very strong magnetic fields (7 T), Sugiyama *et al.*[41] and Revol *et al.*[42] showed that CNC cholesteric domains successfully align and form one monodomain structure with their helicoidal axis pointing along the

magnetic field, due to the intrinsic diamagnetic anisotropy of the nanorods.[43] However, magnetic fields only allow orienting the whole cholesteric structure and involves slow relaxation times of several hours,[44] while not providing further control on the cholesteric periodicity of the phase. Local magnetic alignments in lower fields have since then been reported in bulk suspensions with no obvious change of the optical properties. Using electric fields, Bordel *et al.* showed that cellulose fibers in apolar solvents align parallel to the applied field,[45] while an oriented nematic ordering was reported by Habibi *et al.* on individual CNCs, as observed on a suspension left drying on a micron-scaled electric junction.[46] Using diluted CNC suspensions in apolar solvents, we revealed that this electric field coupling is due to the presence of both permanent and induced dipole moments on individual CNCs,[47] while Oulachgar *et al.* illustrated further their utilization as electro-optical spatial light modulator.[48] Electric and magnetic field alignment of other colloidal liquid crystals have been widely studied.[49-56] Earlier, Dogic and Fraden[57] showed that colloidal liquid crystals made of chiral fd-viruses present a transition from cholesteric to nematic when a continuous magnetic fields is applied. Interestingly, Chiba *et al*. reported the electro-optical behavior of aqueous solution of hydroxypropyl cellulose (HPC), a polymeric cellulose derivative forming lyotropic cholesteric phases,[58] but this effect was indirectly due to the introduction of an ionic concentration gradient by the applied DC electric field.[58,59] To the best of our knowledge, no studies of the effect of electric fields on the cholesteric suspension of CNCs or any comparable colloidal cholesteric suspension have been reported so far.

In this work, we demonstrate that electric fields are an efficient and convenient tool to control the iridescence properties of concentrated CNCs in an apolar solvent. This method not only allows a precise tuning of the pitch but also enables sample homogeneity at the macroscopic scale as well as dynamical control of the structural colors. In the following, we first introduce the relevant quantities to consider when controlling the cholesteric phase behavior under an

electric field, and then justify the use of apolar solvent for this system. We utilize qualitative iridescence and quantitative laser diffraction observations to monitor the effect of electric fields on the orientation and periodicity of the cholesteric phase, as they are strongly related to the optical properties of the sample. We confront our observation to existing models to test our suggested scenario and also derive from it the twisting constants characterizing this phase. Finally, we address the relevance of this tool to manipulate the cholesteric order to either increase its ordering after field removal or by controlling it over time to dynamically tune its resulting iridescence.

The cholesteric phase is characterised by a local ordering of the CNCs within *cholesteric domains*, where the rods spontaneously align along a common direction called the director, $\boldsymbol{n}$, which locally rotates and describes a left-handed helix about an axis, $\boldsymbol{h}$. The distance that separates rods of same orientation after a 360° rotation is commonly defined as the cholesteric pitch of the helix, p.[60]

Due to CNC birefringence, light is diffracted by the cholesteric structure in the plane defined by the incident beam and the helix $\boldsymbol{h}$, at an angle θ according to Bragg's law. This causes both strong iridescence of the samples and the diffraction pattern from a monochromatic laser beam (cf. Supporting Information, **Figure 1a-b** and **Figure S1**). The diffraction pattern corresponds to the observation of the sample reciprocal space: the direction of the observed peaks corresponds to the projection of $\boldsymbol{h}$ while the radial peak position gives access to p. Noteworthy, this situation differs from solid cholesteric films obtained by slowly drying CNC suspension, as the much larger pitches involved here, prior to any pitch collapse upon drying, lead to the diffraction of visible light at much smaller θ angles, justifying a sample illumination in transmission and not in reflection.

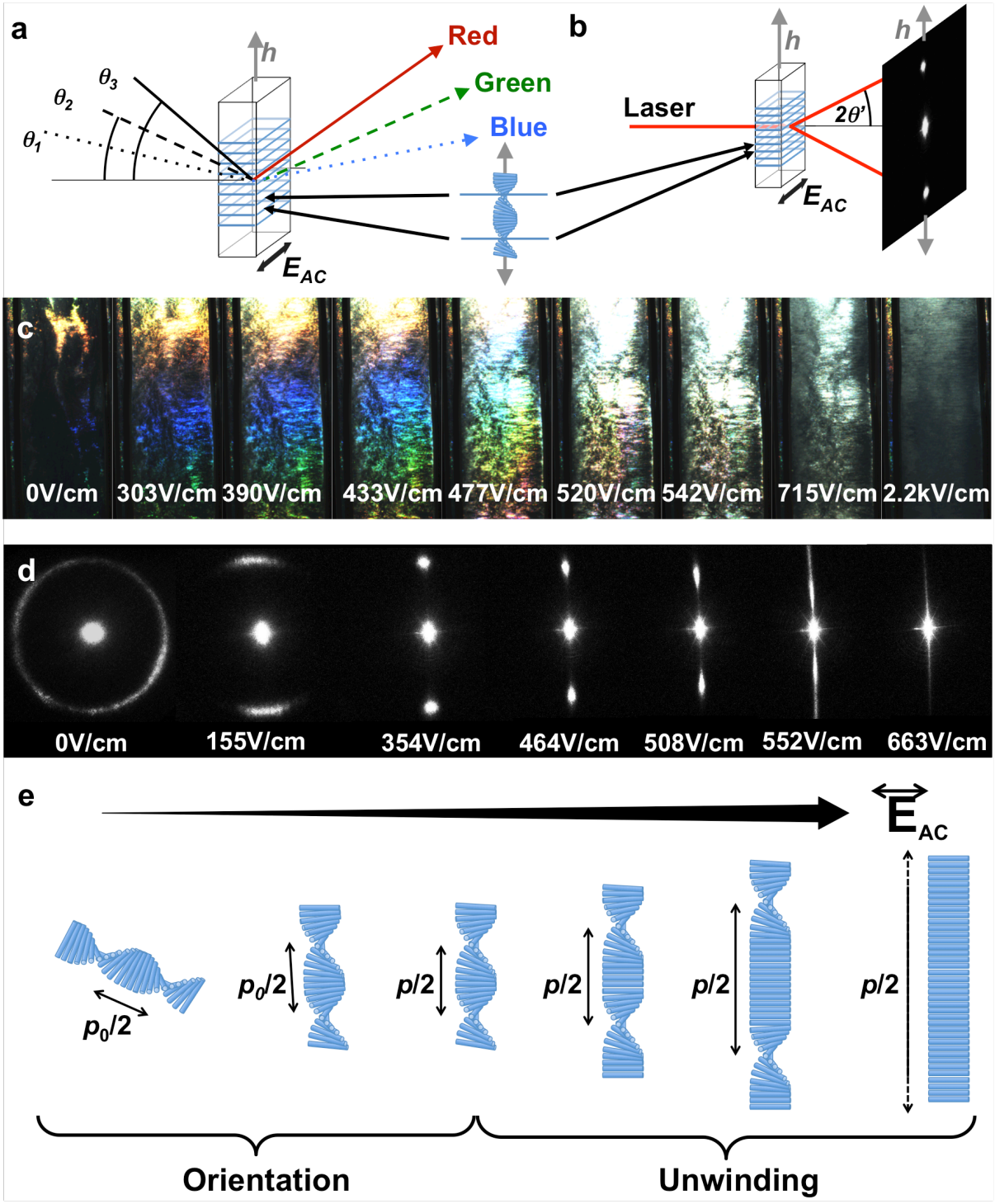

Figure 1. (a-b) Schematics illustrating (a) iridescence and (b) laser diffraction as effects of the same light diffraction caused by the underlying cholesteric structure; the geometry of the field direction, an example of cholesteric monodomain and its corresponding diffraction peaks position is indicated in (b). (c) Iridescence evolution of a polydomain cholesteric sample upon first electric field application (values in rms), displaying increase of light intensity, then

red-shift and finally color desappearance. (d) Evolution of the laser diffraction pattern upon electric field increase, showing cholesteric orientation, then pitch increase and finally complete cholesteric unwinding. (e) Schematic of the sequential cholesteric orientation and unwinding upon electric field increase.

The CNCs used here were dispersed in an apolar solvent (toluene), which offers a number of advantages over aqueous media.[61,62] First, surfactant-coated CNCs in toluene self-assemble into a cholesteric phase at concentrations as high as 35 wt%, whereas aqueous dispersions get trapped into a glassy/gel phase above ~15 wt%.[63,64] Second, a better index-matching reduces Rayleigh scattering, increases the transparency and enhances the light diffraction due to CNC intrinsic birefringence. This index-matching also minimizes the dispersion forces contributing to van der Waals interactions: this leads to successful stabilization with surfactants without the need of an extended electrostatic double-layer as required in aqueous suspension. As a result, the rod concentration can be increased without aggregating or jamming into a Wigner glass.[65] Third, the apolar solvent enables using high voltages and thus strong electric fields on large distances in the suspension to align the CNCs parallel to the electric field, as shown with CNCs extracted from tunicate.[45]

The effect of an increasing electric field on the iridescence of a fully cholesteric CNC suspension is presented in **Figure 1c**. The sample was placed in a glass capillary held vertically with two metallic electrodes connected to a high AC voltage source operating at 1 kHz, and a white light source was placed in the sample background, slightly off-centered vertically with respect to the viewing angle of the camera. At low field value, a clear increase in the light intensity is first observed, followed by a red-shift of the color. At higher fields, the color turned into a scattering white and finally vanished. Before turning transparent, the sample presented an inhomogeneous aspect due to its polydomain nature, while the

homogeneous aspect at the highest field indicated a total alignment of the CNCs parallel to the applied field into a so-called paranematic phase.

Monochromatic laser diffraction[64,66,67] of the same sequence was then used to extract quantitative information about the cholesteric arrangement, as illustrated in **Figure 1b-1d**.

At zero field, the diffraction pattern appears circular, indicating a multidomain structure of isotropically-distributed cholesteric domains of constant pitch. As the electric field is increased, the diffraction ring evolves towards two symmetric arches of decreasing angular width, in agreement with a progressive orientation of the cholesteric domains perpendicular to the field ($h \perp E$). The alignment of the diffracting domains leads to directional iridescence, with an increase of light intensity, as aforementioned. At larger fields, the radius of the diffraction peaks decreases, indicating an increase of the pitch, p. As the field further increases, the peaks broaden and do not allow to define p anymore, until the whole diffraction pattern vanishes and only the transmitted incident beam remains visible, in agreement with the observed sample transparency (cf. full sequence in **Figure S3**). These observations strongly support the scenario illustrated in **Figure 1e** where the electric field first orients and then unwinds the cholesteric structure.[68-72]

Quantitative modeling of this cholesteric unwinding can be extracted and related to the long-lasting question of the nature of chiral interactions between CNCs.[19,73-80] Due to the lyotropic nature of these liquid crystals, concentration strongly impacts their final properties. We therefore prepared samples of increasing CNC concentrations (from 13 wt% to 38 wt%, cf. **Table S1**), covering the concentration of isotropic-anisotropic coexistence domain (cf. **Figure S2**), and we investigated their behavior under electric fields. The pitch evolution *versus* electric field is reported in **Figure 2a** and shows for each investigated concentration a divergence of the pitch when the field is increased. Data were compared to the model initially developped by de Gennes for the unwinding of a molecular cholesteric liquid crystal under a magnetic field,[68] solved for the case of negligible confinement[81] when the twist energy

density is smaller than the bend energy density ($K_{22} < K_{33}$),[71] and that we adapted to electric fields (cf. modeling in SI, **Section C**). The good agreement between the model and the experimental data provides us with reliable values for p_0, the pitch in zero field, and E_c, the critical electric field, extracted as fitting parameters and displayed in **Figure 2b-c**.

From these parameters we can extract the ratio $K_{22}/\Delta\chi_{susp}$ between the twist energy density K_{22} of the cholesteric phase and the local anisotropic dielectric susceptibility $\Delta\chi_{susp}$ of the suspension. From the electric field-induced birefringence of the CNC suspension in diluted suspension (cf. **SI**, **Section D** and **Figure S4**), we estimated $\Delta\chi_{susp}$ and therefore the twist constant K_{22} of the cholesteric phase and its twisting power $K_t = 2\pi K_{22}/p$ on a range of CNC concentrations (**Figure 2e-f**; for a volume fraction Φ ~ 20-35%, K_{22} ~ 0.02-0.07 pN, K_t ~ 0.03-0.2 pN/µm). Interestingly, our system compares well with fd-virus suspensions[57] in the limit of high screening charge and high rod concentration (cf. **SI, Section E** and **Figure S5**). This tendency does not favor the explanation of the chiral twist as an helicoidal charge distribution on the twisting colloids, as the dielectric constant of toluene does not allow a sufficient ionic dissociation and hence impedes electrostatic interactions.

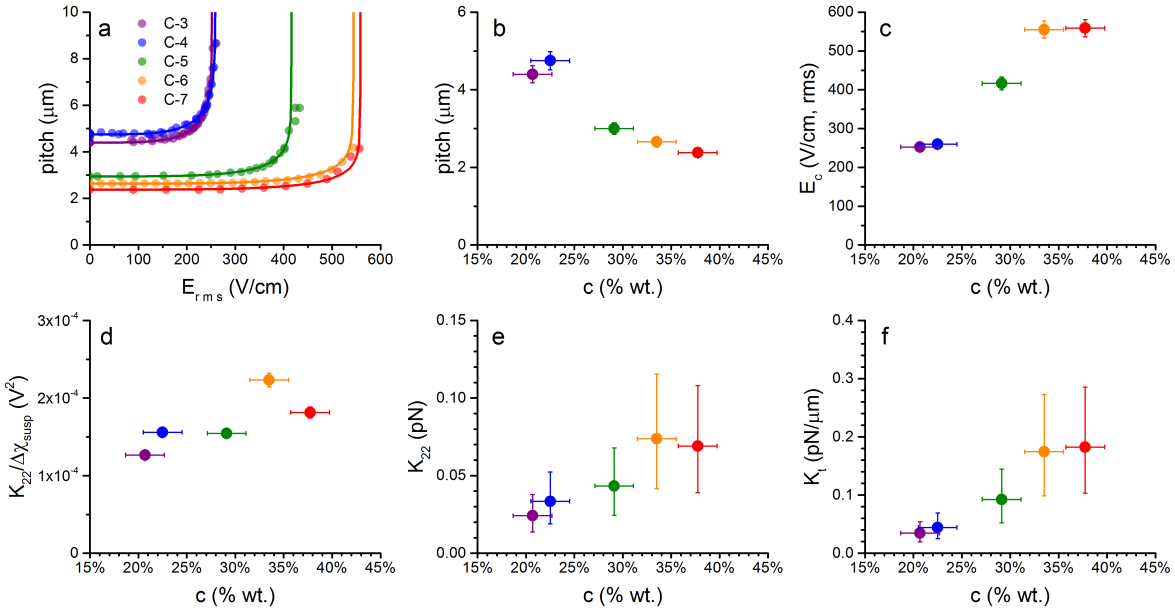

Figure 2. Quantitative analysis of the pitch unwinding under electric field: (a) pitch dependence with applied electric field (symbols) and corresponding fits from de Gennes

model (lines); (b-c) pitch value p_0 at zero field and critical electric field E_c as extracted from the fits. (d) ratio $K_{22}/\Delta\chi$ as extracted from de Gennes theory. (e-f) Using the $\Delta\chi$ estimation from birefringence measurements, we can estimate the twist energy K_{22} and twisting power $K_t = 2\pi K_{22}/p_0$ of the liquid crystalline phase.

Beyond the control of the pitch and the possibility to frustrate thermodynamics to create a paranematic phase, reaching sample homogeneity at the macroscopic scale is a major challenge that was addressed by dynamic actuation using modulated electric fields.

We introduce as *electric field annealing* a treatment corresponding to the application of an electric field sequence in time (**Figure 3)** in order to affect the final sample structure, in a similar way as other types of annealing such as thermal or osmotic. Starting from either an inhomogeneous polydomain or a more organized cholesteric CNC suspension, a strong electric field, i.e. above the critical E_c field, is first applied to melt the cholesteric structure and its existing defects, in order to obtain a fully unwound structure. Then, two different situations were investigated.

First, in the *fast annealing* treatment, the electric field was suddenly removed (**Figure 3a**). Under such conditions, the cholesteric structure rapidly reappears, as indicated by the observation of a uniform diffraction ring within a few minutes (**Figure 3b**). The sample obtained after such treatment thus displays disoriented cholesteric domains. This randomized structure is observed even when applied to a previously well oriented cholesteric sample (cf. **SI, Section F** and **Figure S6-S7**).

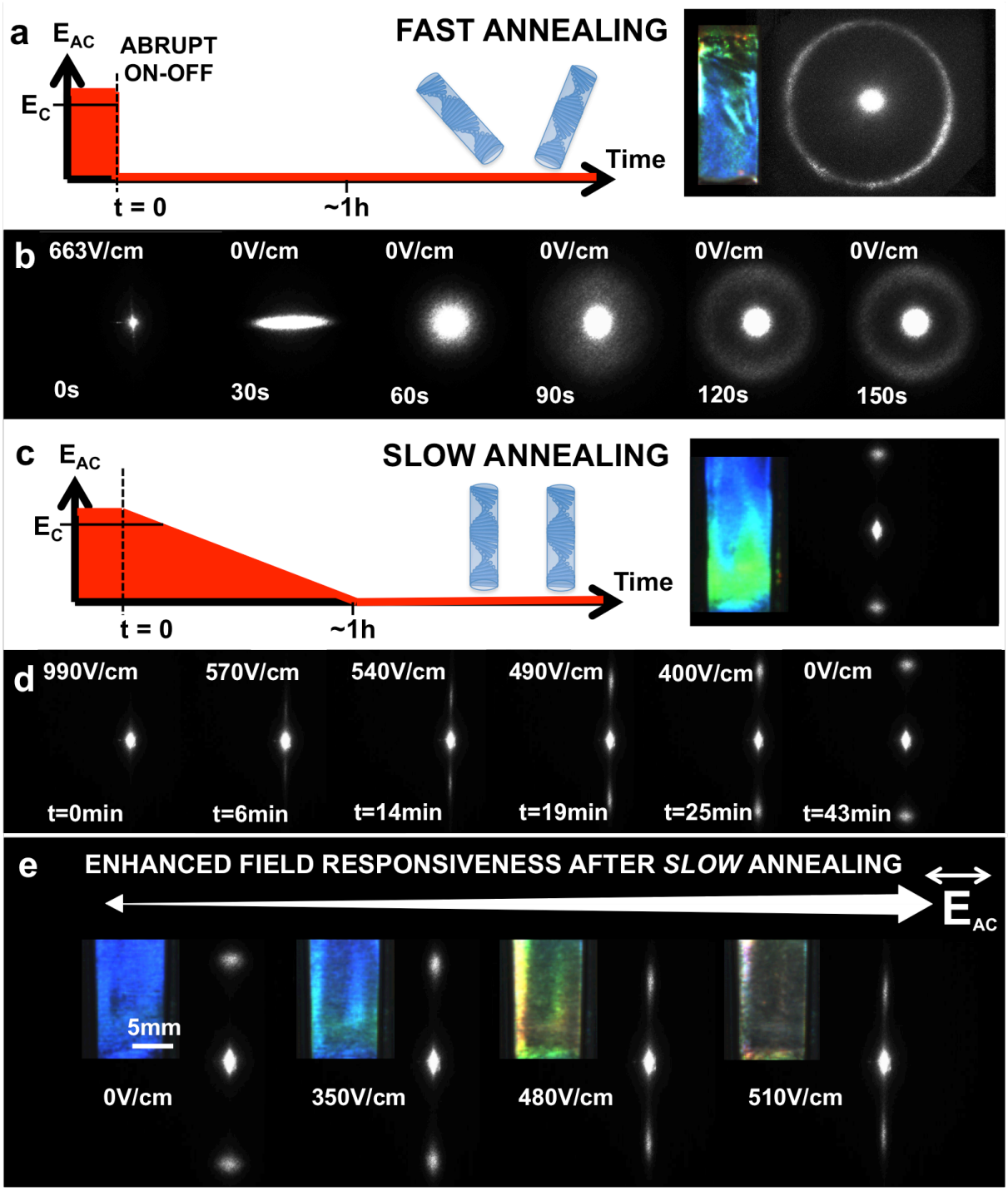

Figure 3. *Fast annealing* versus *slow annealing* in controlling the macroscopic structure of the cholesteric sample and its enhanced responsiveness: (a) Schematic of *fast annealing* method. The inserts display randomized orientation of the cholesteric domains, inhomogeneous iridescent texture and diffraction ring. (b) Laser diffraction recorded during the *fast relaxation* towards a polydomain cholesteric structure. (c) Schematic of *slow annealing* method. The inserts display oriented cholesteric domains, homogeneous iridescent

texture and monodomain diffraction peaks. (d) Laser diffraction recorded during the slow relaxation towards an oriented cholesteric structure. (e) Enhanced field responsiveness of the sample after slow annealing treatment, displaying control of the uniform iridescent texture with the applied field. (NB: apparent color gradient is due to parallax effects in the observation geometry).

Second, in the *slow annealing* treatment, a progressive decrease of the electric field within ~45 min was applied, as illustrated in **Figure 3c**. This treatment led to a much more organized structure as the cholesteric phase was given enough time to rewind with its helix axis perpendicular to the electric field (**Figure 3d**), breaking the symmetry of the cholesteric reformation. The iridescence of the sample after slow annealing appears homogeneous on the centimeter lengthscale and the diffraction pattern indicates a well defined orientation of the monodomain. The diffraction patterns observed in the decreasing sequence indicates a reversible pitch value with little hysteresis, while the orientation of the cholesteric is dramatically enhanced (cf. **SI, Section G** and **Figure S8-S9**). This slow annealing using electric field enables us to obtain high quality orientation and uniform iridescence across a centimeter large sample, which is extremely valuable for such biosourced systems made of highly polydisperse nanocolloids, and relevant for structuration of nanocomposites in material applications. Moreover, the enhanced responsiveness of our system to electric fields after slow annealing treatment allows us to obtain a highly homogeneous colloidal liquid crystal with electric field tunable iridescence, as illustrated in **Figure 3e**.

The dynamic control of the iridescence using a time-modulated electric field was subsequently investigated, i.e. using 1 kHz AC electric field as before but combining sequences of two different amplitudes over time, both kept below the critical E_c value. As shown in **Figure 4a-b**, the iridescent colour of the sample can be dynamically tuned using an electric field amplitude modulated on the timescale of a few seconds, i.e. at modulating

frequencies below ~0.15 Hz (cf. **Video S1**). The corresponding diffraction pattern showed pitch oscillations with no significant broadening of the diffraction peaks (cf. **Video S2**), demonstrating the dynamic tunability of the structure and the iridescence with the electric field.

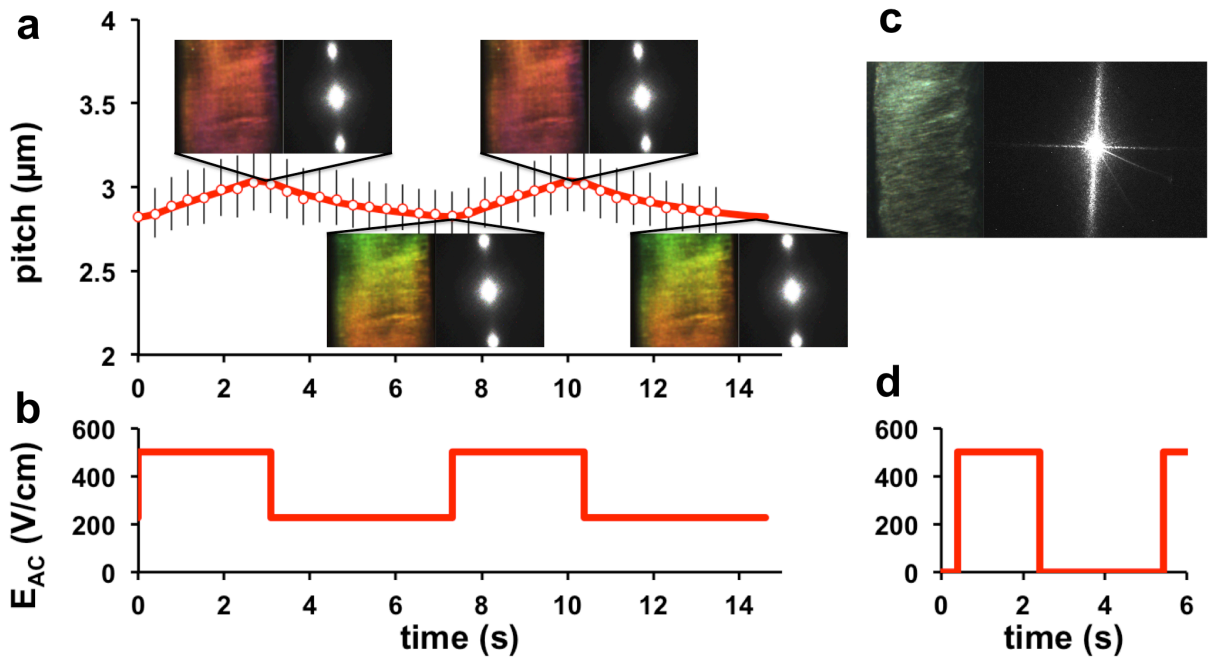

Figure 4. Dynamic control of the sample iridescence with time-modulated electric field (AC 1 kHz) after *slow annealing*: (a-b) example of steady-state dynamic pitch control when electric field is time-modulated. Inserts display on the left the alternated red-shift and blue-shift, and on the right the corresponding diffraction peaks. (c) Example of *structural-white* (broadening of the iridescent colors over the full visible range) with (d) a diffraction line indicating no clearly defined pitch, obtained for AC fields modulated at faster pace and larger amplitudes.

Additional conformation can be achieved using dynamic modulation of the electric field amplitude. When the field is suddenly increased above the critical electric field value E_c, the sample iridescence first turns into a transient white and eventually disappears after few seconds in a perfectly transparent sample. The diffraction pattern corresponding to this

transient white scattering is a continuous line where light is scattered across a large angular window perpendicular to the field. Interestingly, such structural white can be obtained in steady-state under a dynamic modulation of the electric field when modulated over time between more extreme electric field values at higher modulating frequencies, e.g. when alternating between E = 1.5 E_c and 0 V/cm at 0.5 Hz (**Figure 4c-d**). This last configuration provides an example of steady-state dynamic self-assembly[82] and further illustrates the high degree of tunability offered by utilizing electric fields on CNCs.

In summary, we have shown that cellulose nanocrystals suspension in apolar solvent can be manipulated with electric fields to finely tailor their self-assembly into iridescent chiral nematic phases with a surprising effectiveness. First, we were able to control the orientation of the cholesteric phase at low electric field, the tuning of the iridescence at intermediate fields, and the formation of a purely nematic phase at higher fields. Second, we quantified the critical electric field at which the unwinding of the cholesteric occurs, from which we estimated the K_{22} twisting energy density of the cholesteric phase. Third, we introduced the effect of electric field annealing treatment using either a fast or slow field loop to produce highly disoriented or uniformly oriented cholesteric phases in zero field. Fourth, we showed that time-modulated electric fields enables dynamic color changes when the field is varied at low frequencies (f < 0.1 Hz), while a faster and larger electric field modulation produces a switchable steady-state *structural-white* scattering sample. The simple and effective electric-field manipulation of colloidal liquid crystals described here provides an enhanced control over the structures and associated properties and adds to the *self-assembly toolbox* as a multi-purpose plateform. Recently, electric control of colloidal particle arrangement immersed into cholesteric liquid crystals showed strong hysteresis behavior, enabling the bistability required for energy-saving liquid crystalline displays.[83-86] As for this example, our work paves the

way to applications in responsive and tunable systems, as well as in the design of ordered nanocomposite materials.

Experimental

Preparation of CNC suspension in water. An aqueous CNC suspension was obtained from the acid hydrolysis of cotton linters in 64 wt% sulfuric acid for 30 min at T = 63 °C, following the method[42] initially described by Revol *et al.* The suspensions were washed by repeated centrifugation/redispersion steps, dialyzed against distilled water until constant conductivity of the dialysis bath and ultrasonicated for 4 min (Branson Digital sonifier 450). After filtration (0.8 μm, cellulose nitrate membranes, Sartorius), stable aqueous suspensions of rod-like CNCs were obtained (cf. **Figure S10**). Conductometric titration[87] against NaOH was used to quantify the functionalization with $–OSO_3^-$ groups of the resulting CNCs and led to 181 mmol S/kg (i.e. [S] ~ 0.58 wt%).

Transmission Electron Microscopy (TEM) of CNCs. As described elsewhere,[88] a droplet of ca. 0.001 wt% CNC aqueous suspension was deposited on a freshly glow-discharged carbon-coated TEM copper grid. The excess liquid was blotted with filter paper and the remaining film was allowed to dry. The specimen was observed under low dose illumination in a Philips CM200 microscope (FEI) operating at 200 kV. The images were recorded using a F216 TVIPS digital camera.

Preparation of CNC suspensions in toluene. CNC suspensions in toluene were obtained by adding Beycostat NA surfactant (BNA, CECCA-ATO Co), a phosphoric ester of polyoxyethylene(9) nonylphenyl ether, with a surfactant/CNC ratio of 4/1 (w/w) to the aqueous CNC dispersion. After freeze-drying, two cycles of redispersion in toluene followed by centrifugation were applied as described elsewhere[61] to yield a concentrated pellet free of surfactant excess.

To produce a 40 wt% concentrated homogeneous stock suspension, some paste was redispersed in toluene using a planetary centrifugal mixer (Thinky Mixer ARE-250, Poly Dispensing System). Investigated samples resulted from the dilution of this stock suspension. The CNC mass concentration c is measured in terms of dry mass residue and can be related to its volume fraction, Φ (cf. SI, Section A).

Preparation of electric field cuvettes. Square profiled borosilicate glass capillaries (CM Scientific Rect. Boro Capillaries, #4410-100, internal dim. 100x10x1.0 (in mm), external width 11.5 mm) were split in two halves under acetylene flame, and a pair of stainless steel wires (diameter 0.9 mm) were inserted inside each half-capillary in order to be used as electrodes. One end was kept open while the other capillary end was sealed with acetylene flame. Terminal blocks connectors were mounted on the wire ends to allow easy and secure connection with the high voltage source.

The cuvette was filled with the sample and sealed using fast drying epoxy resin. A small amount of the remaining sample was used to double-check the final sample concentration. The samples were left at rest in these cuvettes for at least 48 h prior to any experiment in order to allow phase separation to occur.

The sample structural order was probed by its optical properties, using several different settings, including direct observation, observation between crossed polarizers and light diffraction methods, as described in Supporting Information.

Supporting Information

The supporting information are available free of charge on Wiley-VCH website and include:

A. Sample preparation, phase transition properties (isotropic-cholesteric phase diagram, cholesteric pitch determination) and investigation methods;
B. Sample orientation under electric field;
C. Modeling of the cholesteric unwinding (*de Gennes* theory);
D. Static Electric Birefringence in diluted suspension;

E. Comparison of CNC liquid crystalline properties with fd-virus suspensions;

F. Sample relaxation under electric field fast annealing;

G. Sample relaxation under of electric field slow annealing

H. Transmission Electron Microscopy (TEM) image of the CNCs used

Author Information

Present address. B.F.-P.: Melville laboratory for Polymer synthesis, Department of Chemistry, University of Cambridge, UK.

Note. The authors declare no competing financial interest.

Acknowledgements

The authors thank Jean-Luc Putaux for TEM imaging and Jérémy Astruc for optical microscopy, Pierre Sailler and Patrice Ballet for technical assistance, and B.F-P. thanks Richard M. Parker and Silvia Vignolini for valuable discussions. The authors acknowledge funding by the French National Research Agency under grant agreement ANR-08-NANO-P235-36 and B.F.-P acknowledges the Travel Grant COST-STSM-FP1205-30247.

Received: ((will be filled in by the editorial staff))
Revised: ((will be filled in by the editorial staff))
Published online: ((will be filled in by the editorial staff))

References

[1] H. Ghiradella, *Appl. Opt.* **1991**, *30*, 3492.
[2] A. E. Seago, P. Brady, J. P. Vigneron, T. D. Schultz, *J. R. Soc. Interface* **2009**, *6*, S165.
[3] V. Sharma, M. Crne, J. O. Park, M. Srinivasarao, *Science* **2009**, *325*, 449.
[4] L. Poladian, S. Wickham, K. Lee, M. C. J. Large, *J. R. Soc. Interface* **2009**, *6*, S233.
[5] G. E. Schröder-Turk, S. Wickham, H. Averdunk, F. Brink, J. D. Fitz Gerald, L. Poladian, M. C. J. Large, S. T. Hyde, *J. Struct. Biol.* **2011**, *174*, 290.
[6] S. Vignolini, E. Moyroud, B. J. Glover, U. Steiner, *J. R. Soc. Interface* **2013**, *10*, 20130394.
[7] S. Vignolini, P. J. Rudall, A. V. Rowland, A. Reed, E. Moyroud, R. B. Faden, J. J. Baumberg, B. J. Glover, U. Steiner, *Proc. Natl. Acad. Sci. USA* **2012**, *109*, 15712.
[8] M. Srinivasarao, *Chem. Rev.* **1999**, *99*, 1935.
[9] P. Vukusic, J. R. Sambles, *Nature* **2003**, *424*, 852.
[10] B. Bhushan, *Phil. Trans. R. Soc. A.* **2009**, *367*, 1445.
[11] Y. Fu, C. A. Tippets, E. U. Donev, R. Lopez, *Wiley Interdiscip. Rev. Nanomed.*

Nanobiotechnol. **2016**, *8*, 758.
[12] Z. Han, Z. Mu, W. Yin, W. Li, S. Niu, J. Zhang, L. Ren, *Adv. Colloid Interface Sci.* **2016**, *234*, 27.
[13] A. G. Dumanli, T. Savin, *Chem. Soc. Rev.* **2016**, *45*, 6698.
[14] Y. Habibi, L. A. Lucia, O. J. Rojas, *Chem. Rev.* **2010**, *110*, 3479.
[15] C. Salas, T. Nypelö, C. Rodriguez-Abreu, C. Carrillo, O. J. Rojas, *Curr. Opin. Colloid Interface Sci.* **2014**, *19*, 383.
[16] J. P. F. Lagerwall, C. S. U. tz, M. Salajkova, J. Noh, J. H. Park, G. Scalia, L. B. O. m, *NPG Asia Materials* **2014**, *6*, e80.
[17] M. Giese, L. K. Blusch, M. K. Khan, M. J. MacLachlan, *Angew. Chem. Int. Ed.* **2015**, *54*, 2888.
[18] J. F. Revol, H. Bradford, J. Giasson, R. H. Marchessault, D. G. Gray, *Int. J. Biol. Macromolec.* **1992**, *14*, 170.
[19] Xue Min Dong, Tsunehisa Kimura, A. Jean-François Revol, D. G. Gray, *Langmuir* **1996**, *12*, 2076.
[20] T.-D. Nguyen, B. U. Peres, R. M. Carvalho, M. J. MacLachlan, *Adv. Funct. Mater.* **2016**, *26*, 2875.
[21] Y. Zhang, O. Paris, N. J. Terrill, H. S. Gupta, *Scientific Reports* **2016**, *6*, 26249.
[22] X. Mu, D. G. Gray, *Langmuir* **2014**, *30*, 9256.
[23] J.-F. Revol, D. L. Godbout, D. G. Gray, *Solidified Liquid Crystals of Cellulose with Optically Variable Properties*, **1997**, US5629055 A.
[24] S. Beck, J. Bouchard, R. Berry, *Biomacromolecules* **2011**, *12*, 167.
[25] R. Bardet, F. Roussel, S. Coindeau, N. Belgacem, J. Bras, *Carbohydr. Polym.* **2015**, *122*, 367.
[26] G. Guidetti, S. Atifi, S. Vignolini, W. Y. Hamad, *Adv. Mater.* **2016**, DOI 10.1002/adma.201603386.
[27] S. N. Fernandes, P. L. Almeida, N. Monge, L. E. Aguirre, D. Reis, C. L. P. de Oliveira, A. M. F. Neto, P. Pieranski, M. H. Godinho, *Adv. Mater.* **2016**, DOI 10.1002/adma.201603560.
[28] K. E. Shopsowitz, H. Qi, W. Y. Hamad, M. J. MacLachlan, *Nature* **2010**, *468*, 422.
[29] J. A. Kelly, A. M. Shukaliak, C. C. Y. Cheung, K. E. Shopsowitz, W. Y. Hamad, M. J. MacLachlan, *Angew. Chem. Int. Ed.* **2013**, *52*, 8912.
[30] M. Giese, L. K. Blusch, M. K. Khan, W. Y. Hamad, M. J. MacLachlan, *Angew. Chem.* **2014**, *53*, 8880.
[31] Y. P. Zhang, V. P. Chodavarapu, A. G. Kirk, M. P. Andrews, *Sens. Actuator B-Chem.* **2013**, *176*, 692.
[32] Q. Liu, M. G. Campbell, J. S. Evans, I. I. Smalyukh, **2014**, *26*, 7178.
[33] A. Querejeta-Fernández, G. Chauve, M. Méthot, J. Bouchard, E. Kumacheva, **2014**, *136*, 4788.
[34] A. Lukach, H. Thérien-Aubin, A. Querejeta-Fernández, N. Pitch, G. Chauve, M. Méthot, J. Bouchard, E. Kumacheva, *Langmuir* **2015**, *31*, 5033.
[35] A. Querejeta-Fernández, B. Kopera, K. S. Prado, A. Klinkova, M. Méthot, G. Chauve, J. Bouchard, A. S. Helmy, E. Kumacheva, *ACS Nano* **2015**, *9*, 10377.
[36] P.-X. Wang, W. Y. Hamad, M. J. MacLachlan, *Nat. Commun.* **2016**, *7*, 11515.
[37] Y. Nishiyama, S. Kuga, A. Wada Masahisa, O. Takeshi, *Macromolecules* **1997**, *30*, 6395.
[38] J. A. Diaz, X. Wu, A. Martini, J. P. Youngblood, R. J. Moon, *Biomacromolecules* **2013**, *14*, 2900.
[39] J. H. Park, J. Noh, C. Schütz, G. Salazar-Alvarez, G. Scalia, L. Bergström, J. P. F. Lagerwall, *ChemPhysChem* **2014**, *15*, 1477.
[40] M. Ličen, B. Majaron, J. Noh, C. Schütz, L. Bergström, J. Lagerwall, I. Drevenšek-

Olenik, *Cellulose* **2016**, *23*, 3601.
[41] J. Sugiyama, H. Chanzy, G. Maret, *Macromolecules* **1992**.
[42] J.-F. Revol, L. Godbout, X. M. Dong, D. G. Gray, H. Chanzy, G. Maret, *Liquid Crystals* **1994**, *16*, 127.
[43] B. Frka-Petesic, J. Sugiyama, S. Kimura, H. Chanzy, G. Maret, *Macromolecules* **2015**, *48*, 8844.
[44] K. J. De France, K. G. Yager, T. Hoare, E. D. Cranston, *Langmuir* **2016**.
[45] D. Bordel, J. L. Putaux, L. Heux, *Langmuir* **2006**, *22*, 4899.
[46] Y. Habibi, T. Heim, R. Douillard, *J. Polym. Sci. Part B Polym. Phys.* **2008**, *46*, 1430.
[47] B. Frka-Petesic, B. Jean, L. Heux, *EPL* **2014**, *107*, 28006.
[48] H. Oulachgar, M. Bolduc, G. Chauve, Y. Desroches, P. Beaupre, J. Bouchard, P. Galarneau, *MRS Adv.* **2015**, *1*, 631.
[49] B. J. Lemaire, P. Davidson, D. Petermann, P. Panine, I. Dozov, D. Stoenescu, J. P. Jolivet, *Eur. Phys. J. E* **2004**, *13*, 309.
[50] G. Filipcsei, I. Csetneki, A. Szilágyi, M. Zrínyi, in *Oligomers, Polymer Composites, Molecular Imprinting*, Springer Berlin Heidelberg, Berlin, Heidelberg, **2007**, pp. 137–189.
[51] J. Fresnais, J. F. Berret, B. Frka-Petesic, O. Sandre, R. Perzynski, *Adv. Mater.* **2008**, *20*, 3877.
[52] M. E. Leunissen, H. R. Vutukuri, A. van Blaaderen, *Adv. Mater.* **2009**, *21*, 3116.
[53] P. Dommersnes, Z. Rozynek, A. Mikkelsen, R. Castberg, K. Kjerstad, K. Hersvik, J. Otto Fossum, *Nat. Commun.* **2013**, *4*, 2066.
[54] B. Bharti, O. D. Velev, *Langmuir* **2015**, *31*, 7897.
[55] K. May, A. Eremin, R. Stannarius, S. D. Peroukidis, S. H. L. Klapp, S. Klein, *Langmuir* **2016**, *32*, 5085.
[56] M. Wang, Y. Yin, *J. Am. Chem. Soc.* **2016**, *138*, 6315.
[57] Z. Dogic, S. Fraden, *Langmuir* **2000**, *16*, 7820.
[58] R. Chiba, Y. Nishio, Y. Miyashita, *Macromolecules* **2003**, *36*, 1706.
[59] R. Chiba, Y. Nishio, Y. Sato, M. Ohtaki, Y. Miyashita, *Biomacromolecules* **2006**, *7*, 3076.
[60] E. Belamie, P. Davidson, M. M. Giraud-Guille, *J. Phys. Chem. B* **2004**, *108*, 14991.
[61] L. Heux, G. Chauve, C. Bonini, *Langmuir* **2000**, *16*, 8210.
[62] S. Elazzouzi-Hafraoui, J.-L. Putaux, L. Heux, *J. Phys. Chem. B* **2009**, *113*, 11069.
[63] C. Honorato-Rios, A. Kuhnhold, J. R. Bruckner, R. Dannert, T. Schilling, J. P. F. Lagerwall, *Front. Mater.* **2016**, *3*, 75.
[64] R. M. Parker, B. Frka-Petesic, G. Guidetti, G. Kamita, G. Consani, C. Abell, S. Vignolini, *ACS Nano* **2016**, *10*, 8443.
[65] D. Bonn, H. Tanaka, G. Wegdam, H. Kellay, J. Meunier, *EPL* **2007**, *45*, 52.
[66] F. J. Kahn, *Phys. Rev. Lett.* **1970**, *24*, 209.
[67] C. Schütz, M. Agthe, A. B. Fall, K. Gordeyeva, V. Guccini, M. Salajkova, T. S. Plivelic, J. P. F. Lagerwall, G. Salazar-Alvarez, L. Bergström, *Langmuir* **2015**, *31*, 6507.
[68] P. G. de Gennes, *Solid State Commun.* **1968**, *6*, 163.
[69] F. Rondelez, J. P. Hulin, *Solid State Commun.* **1972**, *10*, 1009.
[70] R. Dreher, *Solid State Commun.* **1973**, *13*, 1571.
[71] M. J. Stephen, J. P. Straley, *Rev. Mod. Phys.* **1974**, *46*, 617.
[72] D. Subacius, S. V. Shiyanovskii, P. Bos, O. D. Lavrentovich, *Appl. Phys. Lett.* **1997**, *71*, 3323.
[73] S. J. Hanley, J. F. Revol, L. Godbout, D. G. Gray, *Cellulose* **1997**, *4*, 209.
[74] W. J. Orts, L. G. and, R. H. Marchessault, J. F. Revol, *Macromolecules* **1998**, *31*, 5717.

[75] J. Araki, S. Kuga, **2001**, *17*, 4493.
[76] A. J. Bowling, Y. Amano, R. Lindstrom, R. M. Brown, *Cellulose* **2001**, *8*, 91.
[77] J. F. Matthews, C. E. Skopec, P. E. Mason, P. Zuccato, R. W. Torget, J. Sugiyama, M. E. Himmel, J. W. Brady, *Carbohydr. Res.* **2006**, *341*, 138.
[78] S. Paavilainen, T. Rog, I. Vattulainen, *J. Phys. Chem. B* **2011**, *115*, 3747.
[79] M. Khandelwal, A. Windle, *Carbohydr. Polym.* **2014**, *106*, 128.
[80] S. Dussi, S. Belli, R. van Roij, M. Dijkstra, **2015**, *142*, 074905.
[81] L. M. Blinov, S. P. Palto, *Liquid Crystals* **2009**, *36*, 1037.
[82] G. M. Whitesides, *Science* **2002**, *295*, 2418.
[83] A. Martinez, H. C. Mireles, I. I. Smalyukh, *Proc. Natl. Acad. Sci. USA* **2011**, *108*, 20891.
[84] R. P. Trivedi, I. I. Klevets, B. Senyuk, T. Lee, I. I. Smalyukh, *Proc. Natl. Acad. Sci. USA* **2012**, *109*, 4744.
[85] G. D'Adamo, D. Marenduzzo, C. Micheletti, E. Orlandini, *Phys. Rev. Lett.* **2015**, *114*, 177801.
[86] M. C. M. Varney, Q. Zhang, B. Senyuk, I. I. Smalyukh, *Phys. Rev. E* **2016**, *94*, 042709.
[87] S. Beck, M. Méthot, J. Bouchard, **2014**, *22*, 101.
[88] M. Kaushik, C. Fraschini, G. Chauve, J.-L. Putaux, A. Moores, in *The Transmission Electron Microscope - Theory and Applications*, InTech, **2015**.

Cellulose nanocrystal suspensions in apolar solvent spontaneously form iridescent liquid crystalline phases but the control of their macroscopic order is usually poor. We demonstrate how the use of electric fields can provide control on the cholesteric orientation and its periodicity, allowing macroscopic sample homogeneity and dynamical tuning of their iridescent hues.

cellulose nanocrystals, cholesteric, electric field, iridescence, colloidal liquid crystals

B. Frka-Petesic*, H. Radavidson, B. Jean, L. Heux

Dynamically Controlled Iridescence of Cholesteric Cellulose Nanocrystal Suspensions using Electric Fields

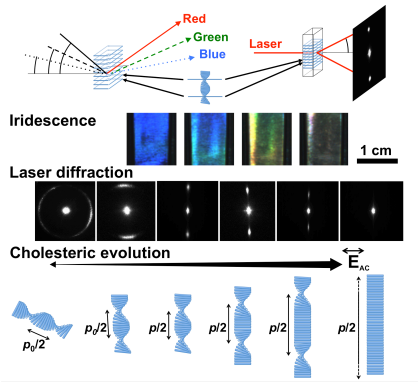

Supporting Information

Dynamically Controlled Iridescence of Cholesteric Cellulose Nanocrystal Suspensions using Electric Fields

Bruno Frka-Petesic, Harisoa Radavidson, Bruno Jean and Laurent Heux*

*corresponding author: bf284@cam.ac.uk

Summary

A. Sample preparation, phase transition properties and investigation methods

In this section we describe how we handle the samples and how they look like under different observation conditions, then we describe the phase transition behavior by showing the phase transition from an isotropic to a cholesteric phase as the concentration is increased. The different settings to probe the optical properties of the samples are also described. Finally the concentration dependence of the pitch of the cholesteric phase, as measured using either local optical microscopy observations or macroscopically averaged laser diffraction technique.

A.1. Sample handling and macroscopic observation

Home-made cuvettes were made from glass capillaries mounted with metallic wires used as electrodes, as shown on **Figure S1a**. The cuvettes were filled with the samples of interest and were left to self-assemble in absence of an electric field. When a phase separation occurred, an isotropic and an anisotropic phase were more easily discriminated by observing the sample between crossed polarizers, as shown on **Figure S1b** and **Figure S1c**.

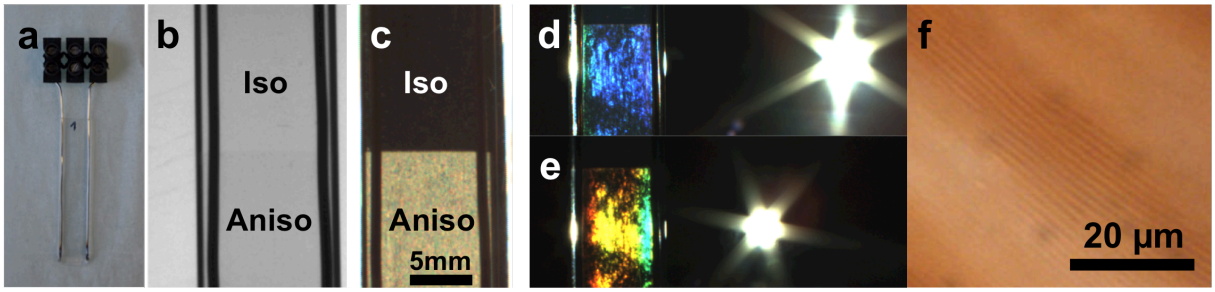

Figure S1. (a) Home-made glass cuvette made from a large glass capillary (ext. width 11.5 mm) and two metallic wires mounted on a choc block, and used as electrodes to apply electric fields on the samples; (b-d) images of different views of a phase-separated sample

(sample A-1) observed (b) with white light backdrop background (c) and between crossed polarizers, or (d-e) localized white light coming from the back at different incident angles, displaying iridescence; (f) optical microscopy observation between crossed polarizers of a sample at 30 wt% showing the fingerprint pattern characteristic of the cholesteric structure (prepared from the batch C) .

The sample reveals vivid iridescent hues in the cholesteric phase only when a localized source of white light is placed in the sample background. The sample color is sensitive to the angle of the incident light, as illustrated in the **Figure S1d** and **Figure S1e**, and to the observation angle. One can note that this sample displays noticeable heterogeneities as it was observed before any electric field was actually applied to the sample.

The cholesteric struture is also confirmed by the direct observation of the characteristic fingerprint pattern as shown in **Figure S1f**, where thin glass capillaries have been used (CM Scientific Rect. Boro Capillaries, #W5010-050, internal dim. in mm: 50x2.00x0.10).

A.2. Overview of prepared samples

The lyotropic nature of the CNC liquid crystalline suspension justified the investigation of their electro-optical properties on a wilder range of CNC concentration, from 100% isotropic to 100% anisotropic. We reported in the **Table S1** the concentration of dry matter c_{dry} and the corresponding volume fraction Φ of the samples investigated in this work. The paste (A, B or C) refers to the batch from which the samples were prepared.

Table S1. List of prepared samples in electrode-containing capillaries with corresponding characteristics.

Sample	Paste	c_{dry} (%wt)	Φ (%vol)	Aniso (%vol)	Pitch (μm)
A-1	A	28.8%	21.3%	70%	4.57
B-1	B	20.2%	14.5%	29%	4.88
C-1	C	2.7%	1.8%	0%	N/D
C-2	C	13.6%	9.5%	0%	N/D
C-3	C	20.7%	14.8%	45%	4.40
C-4	C	22.5%	16.2%	68%	4.75
C-5	C	29.1%	21.5%	100%	3.00
C-6	C	33.5%	25.1%	100%	2.63
C-7	C	37.7%	28.8%	100%	2.38

N/D: the pitch is not defined in a purely isotropic phase.

The concentration were calculated as follow:

The massic ratio of surfactant:CNC has been previously estimated to 0.58:1, equivalent to a massic ratio of m_{CNC}= 1/1.58 ~ 64 wt% of CNC per mass of dry residue.[1] The average density of CNC@BNA is calculated as following:

$$c_{dry} = \frac{\rho_{ave}\,\Phi}{\rho_{ave}\,\Phi+\rho_s(1-\Phi)} \qquad \text{which is equivalent to} \qquad \Phi = \frac{\rho_s\,c_{dry}}{\rho_{ave}-(\rho_{ave}-\rho_s)\,c_{dry}}$$

where ρ_{ave} is defined as the average density of the CNC@BNA:

$$\rho_{ave} = \rho_{CNC}\,\nu_{CNC} + \rho_{surf}(1-\nu_{CNC}) \sim 1.31\ \text{g/cm}^3$$

and the volumc ratio ν_{CNC} is obtained from the massic ratio m_{CNC} as:

$$\nu_{CNC} = \frac{\rho_{surf}\,m_{CNC}}{\rho_{CNC} - m_{CNC}(\rho_{CNC}-\rho_{surf})}$$

Here, ρ_{CNC} = 1.6 g/cm^3 is the density of cellulose, ρ_{surf} is taken as ~1 g/cm^3 and ρ_s = 0.876 g/cm^3 is the density of toluene.

A.3 Isotropic-Cholesteric Phase separation and lyotropic phase diagram

The proportion of anisotropic phase in each sample has been measured by observing the samples in the capillaries in two complementary conditions. The total volume of the sample is measured from a direct observation of the filling level of the capillary in diffuse white light

(i.e. without polarizers, as in Figure S1b – note the sample-air meniscus is not visible in this frame) while the volume of anisotropic phase only is easily determined from an observation between crossed polarizers (as in Figure S1c). The ratio of the volume of anisotropic phase to the total sample volume is reported in **Figure S2**.

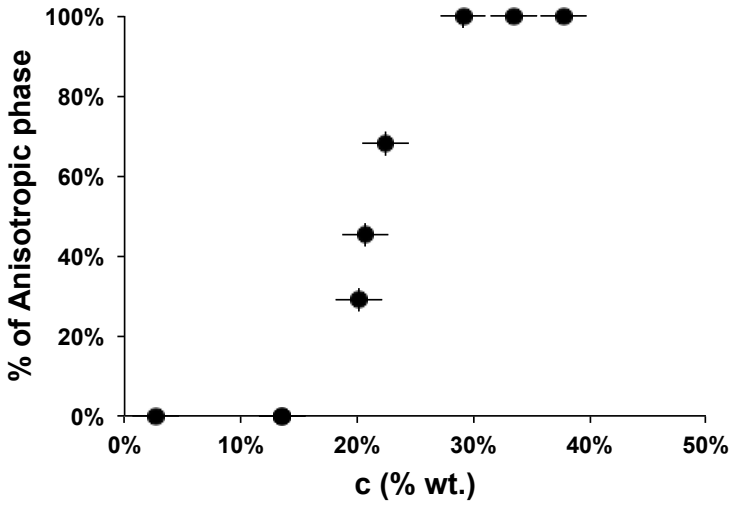

Figure S2. Phase diagram showing proportion of sample volume that turned into an anisotropic phase, for various total CNC concentrations (expressed in wt% of dry matter).

A.4 Direct observation under diffuse white light

The capillary was photographed before applying any electric field using diffuse white light source as a background.

A.5 Observation under Crossed-polarizers against diffuse white light

The sample was inserted between crossed-polarizers oriented at +/-45° with respect to the vertical/horizontal axes and observed with similar observation conditions.

A.6 Dynamic control of applied electric field on liquid crystalline samples

The AC electric field was generated with a function generator (Centrad, GF 265) and amplified with a Trek model 10/10B high voltage power amplifier. The applied electric field $E_{AC} = V_{rms}/e$ (defined in V/cm rms) is determined from the gap e between the electrodes and the root-mean-square of the applied voltage V_{rms}.

A.7 Field-controlled iridescence observation

A white light source (Leica CLS100LED, 3000K) was connected to an optical fibre placed behind the sample at an angle between 15° and 35° above or sideway from the viewing direction, at approximately 30 cm away from the sample. A RGB camera (Sony XCD-SX90CR) was either placed at ~5 cm from the sample for an optimal picture resolution or at approximately 20 cm from the sample to reduce the angular size of the sample and therefore color variation due to parallax.

A.8 Field-controlled laser diffraction measurement

A linearly polarized He-Ne laser with a wavelength λ_0 = 632.8 nm was first circularly polarized and collimated before hitting the sample in the capillary. A grid-marked paper screen was placed at a distance L (typically ~ 15 to 20 cm) behind the sample to form the diffraction pattern, whose image was recorded using an 8-bit camera (Sony XCD-SX90CR, monochromatic settings). The distance L was measured with +/-1 mm resolution. The diffraction angle $2\theta'$ (cf. Figure 2b) was obtained from $2\theta' = \arctan(r/L)$, with r the radius of the first order diffraction peak. The images were analyzed using the ImageJ software (http://imagej.nih.gov/ij/).

A.9. Cholesteric pitch determination from laser diffraction measurements

Laser diffraction is a space-averaged technique that allows simultaneously the measurement of the average pitch and the visualization of helix orientation, as light is diffracted within the plan contained by the incident light beam and the helicoidal axis of the cholesteric domains.

The Bragg's law corrected by Snell's law on the sample/air interfaces is given by[2]:

$$\lambda_0 = \tilde{n}\, p \sin\left[\tfrac{1}{2}\arcsin\left(\tfrac{1}{\tilde{n}}\sin 2\theta'\right)\right] \quad \text{(S1)}$$

where λ_0 is the laser wavelength, p the pitch, $\tilde{n}$ the sample average optical index and θ' the diffraction angle, measured as $\theta' = \arctan(r/L)$, where r is the radius of the diffraction peak and L the distance from the sample to the screen. One can note that the optical index of the

glass does not contribute to the Snell law correction, and the impact of the sample thickness is neglected.

The average optical index of the cholesteric medium can be estimated using Bruggeman modeling, as we recently reported for laser diffraction of aqueous CNC suspensions.[3] However, due to the good index-matching of toluene and cellulose, the optical index does not depend much on the CNC concentration and has been taken to $\tilde{n}$ = 1.50 for all samples.

B. Sample progressive orientation under electric field

The initial sample orientation under electric field can be monitored using laser diffraction. The numerous defects in a sample that was never oriented before required slow increase of the electric field, as illustrated on **Figure S3** from sample C-6. However, such progression becomes faster after a slow annealing step, as illustrated in **section E** of the SI.

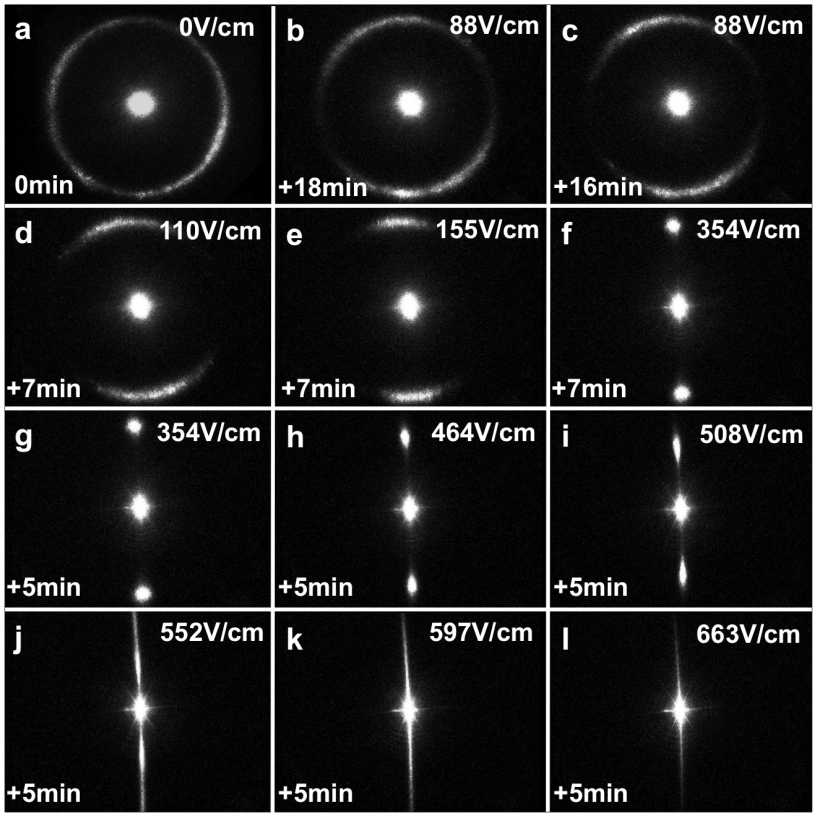

Figure S3. Laser diffraction pattern showing progressive unwinding of the cholesteric under increasing electric field. The duration in the bottom left corner indicated the waiting time from the previous picture and the AC electric field value is given in rms.

C. Modeling of the cholesteric unwinding from *de Gennes* theory

According to de Gennes modeling, the pitch dependence with the electric field value is obtained by introducing a variable k such as for any $k \in [0,1]$:

$$\frac{E}{E_c} = \frac{k}{\boldsymbol{E}(k)} \tag{S5}$$

$$\frac{p}{p_0} = \left(\frac{2}{\pi}\right)^2 \boldsymbol{K}(k)\boldsymbol{E}(k) \tag{S6}$$

with $\boldsymbol{K}(k)$ and $\boldsymbol{E}(k)$ being respectively the complete elliptic integrals of the first and the second kind, and not to be confused with the electric field E and the critical electric field E_c. Using this relations, a parametric plot with k values from 0 ($E = 0$) to 1 ($E = E_c$) allows plotting the $p(E)$ values using just two experimental parameters, the pitch value in zero field p_0 and the critical electric field E_c.

The cholesteric should be totally unwound when the applied electric field E overcomes a critical electric field E_c given by:

$$E_c = \frac{\pi^2}{p_0}\sqrt{\frac{K_{22}}{\Delta\chi_{\text{susp}}}} \tag{S7}$$

where K_{22} is the twist energy constant of the cholesteric, and $\Delta\chi_{\text{susp}}$ is the anisotropic dielectric susceptibility of the concentrated CNC suspension along its local nematic director.

D. Static Electric Birefringence in diluted suspension

D.1. Experimental measurement of field-induced birefringence on diluted samples

The electric field is applied on the sample using a home-made Teflon-based Kerr cell with two glass windows sealed with *Fomblin* (PFPE) grease, with h = 50 mm optical path length and a 5mm gap between metallic electrodes, as described elsewhere[1]. A laser beam of

wavelength λ_0 = 632.8 nm is first polarized at +45° with respect to the electric field direction, then passes through the sample, and again through an analyzer oriented at -45° with respect to the electric field direction, and the transmitted light intensity is recorded with a photodiode. The electric field is here generated by a DAQ-1501 acquisition card (Acquisys) and amplified with a Trek model 10/10B high voltage power amplifier. After each electric field pulse of increasing strength, the actual applied voltage and the photodiode output are measured with the same DAQ-card after either a DC pulse of 200 ms (DC mode) or after applying an AC pulse of 1 s at 1 kHz (AC mode). A second measurement is then performed to check the reproducibility and validate the assumption of equilibrium conditions.

The transmitted light intensity is measured with a photodiode for various electric field values applied in AC or in DC configuration. From the measured intensity, the birefringence Δn is measured using the following formula:

$$I(E) = I_{\min} + [I_{\max} - I_{\min}] \sin^2 \frac{\delta(E)}{2} \tag{S8}$$

$$\Delta n(E) = \frac{\lambda_0 \, \delta(E)}{2\pi \, h} \tag{S9}$$

The birefringence is obtained from the inversion of the sine function using:

$$\delta(E) = \pi \left[\mathrm{k} + \frac{-1+(-1)^k}{2}\right] - 2(-1)^k \arcsin \sqrt{\frac{I(E)-I_{\min}}{I_{\max}-I_{\min}}} \tag{S10}$$

and $k \in \mathbb{N}^*$, an integer starting from k = 1 and incremented by 1 after each passed extremum. The *biref* set-up exists in AC and DC options, and several programs written in *Delphi* were used for data acquisition and processing.

Hereafter, static electric birefringence measurements were performed on sample C-1 and C-2, i.e. in the isotropic regime at different dilutions (cf. sample C-2 on **Figure S4**).

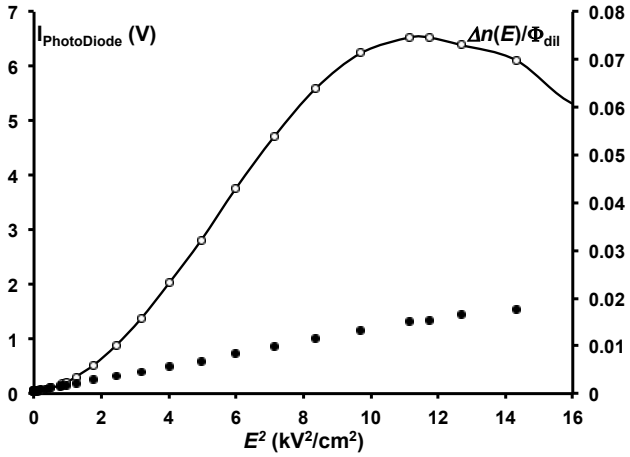

Figure S4. Static Electric Birefringence measured in AC electric field on sample C-1. Open symbols refer to photodiode output (left vertical axis) and closed symbols to birefringence $\Delta n(E)/\Phi_{dil}$ (right vertical axis).

D.2. Modeling of static electric birefringence of individual rods

When an electric field is applied on diluted suspension of colloidal rods in a suspension, the orientation of each individual rod in the steady state is the result of the balance between an electric field torque and the thermal energy k_BT. Due to the anisometric shape of cellulose rods and cellulose intrinsic birefringence, the suspension becomes uniaxially birefringent in the direction of the applied field, and allows measuring the alignment behavior of the rods in the electric field. Therefore, static electric birefringence is sensitive to either permanent or induced electric dipole components as both contribute to the measured birefringence. This technique can be combined to dynamic, or Transient Electric Birefringence to discriminate the permanent and induced components, as recently reported in.[1]

In diluted suspensions, the birefringence of an assembly of rods under electric field can be written as:

$$\Delta n(E) = \delta n_0 \Phi_{dil} S_2(E) \quad \text{(S11)}$$

where δn_0 is the specific birefringence of cellulose nanocrystals in that solvent, Φ_{dil} their volume fraction in the diluted suspension, and $S_2(E)$ is the quadrupolar orientational order parameter of the rods.

In low electric field (i.e. for $\Delta\alpha_{\text{eff}} E^2 << k_B T$), $S_2(E)$ can be expanded to its first order term as the measured birefringence can be written as:

$$S_2(E) = \frac{\Delta\alpha_{\text{eff}} E^2}{15 k_B T} \quad \text{(S12)}$$

with $\Delta\alpha_{\text{eff}} = \Delta\alpha_{\text{i}} + \mu_{\text{p}}^2/k_B T$ defined here as the *effective anisotropic CNC polarizability* containing the sum of any induced and permanent effective components.

Because here $\Delta\alpha_{\text{eff}}$ is an effective anisotropic polarizability of the CNC volume along their long axis, the anisotropic susceptibility $\Delta\chi_{\text{susp}}$ of the suspension containing locally aligned rods can be simply obtained using the following expression:

$$\Delta\chi_{\text{susp}} = \frac{\Delta\alpha_{\text{eff}}}{V}\Phi \quad \text{(S13)}$$

with V being the CNC individual volume and Φ the CNC volume fraction in the investigated anisotropic phase. Combining the previous expression for E_c, one can finally get an expression for the twist energy density K_{22} of the cholesteric phase:

$$K_{22} = \left(\frac{pE_c}{\pi^2}\right)^2 \frac{\Phi}{\Phi_{\text{dil}}} \frac{15}{\delta n_0 V k_B T} \left(\frac{\mathrm{d}\,\Delta n(E)}{\mathrm{d}\,E^2}\right) \quad \text{(S14)}$$

where the slope of $\Delta n(E)$ vs. E^2 is introduced.

E. Comparison of CNC liquid crystalline properties with *fd-virus* suspensions

The pitch p, the twist energy K_{22} and the twisting power K_t are compared to those of cholesteric aqueous suspension of fd-virus extracted from *Dogic et al.*[4]. For the sake of comparison, the data in **Figure S5** are reported using rather the volume fraction Φ obtained using the Equation S4.

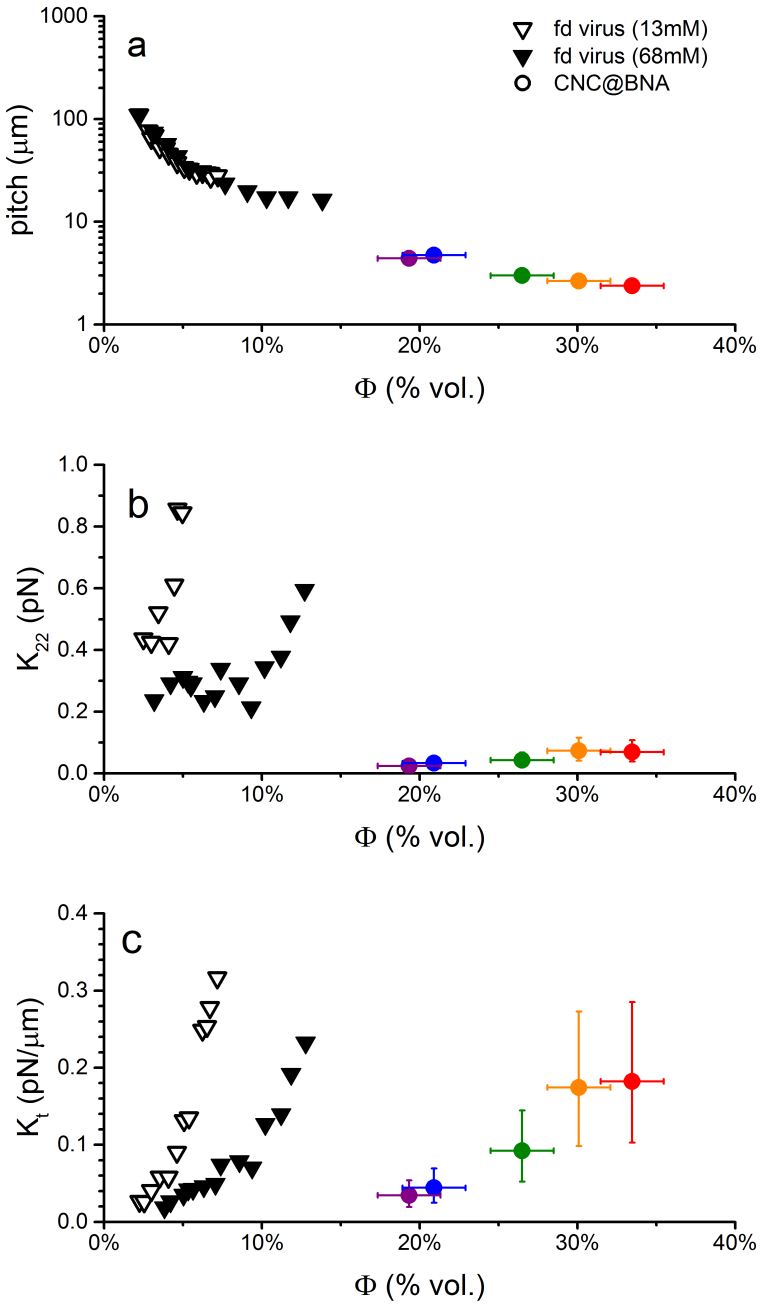

Figure S5. Comparison of the pitch p, the twist energy K_{22} and the twisting power K_t in function of the volume fraction **Φ**, for our system and for fd-virus suspension in 13 mM and 68 mM, according to Dogic *et al.*[4]

F. Sample relaxation under electric field fast annealing (i.e. abrupt field removal)

F.1. Fast annealing relaxation process monitored by laser diffraction

Here, laser diffraction and has been recorded for an abrupt interruption of the electric field, as illustrated on **Figure S6** with laser diffraction relaxation on sample A-1.

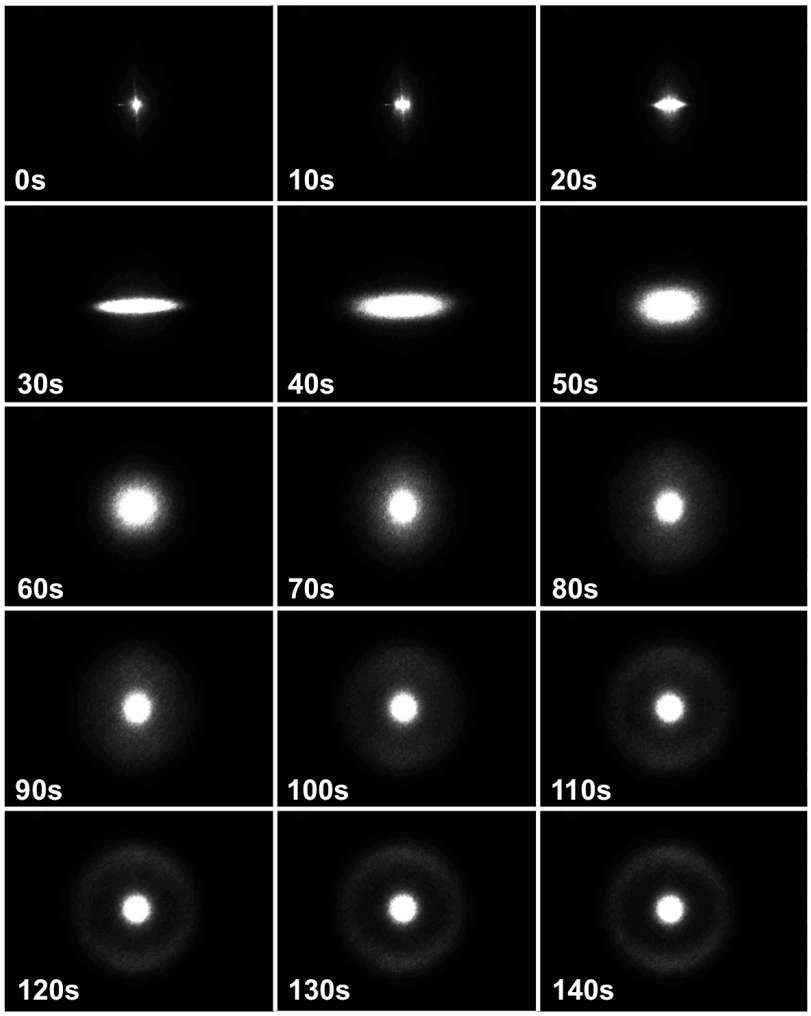

Figure S6. Laser diffraction sequence observed on sample A-1 after abrupt removal of a strong electric field ($E_{t<0}$ = 660 V/cm). After a transient anisotropic pattern, a diffraction ring appeared accounting for cholesteric domains with randomized orientation. Note the timescale in seconds measured from the electric field removal.

The unusual diffraction pattern suggests a transient anisotropic microphase separation along CNC long direction (i.e., along the *E* direction) followed by a relaxation towards a uniform diffraction ring characteristic of a disoriented polycrystalline cholesterics. One can note that

the diffraction ring after 2 minutes is not as sharp as in other measurements as it has not yet reached the final relaxed state (usually about 10-15 min.).

F.2. Fast annealing relaxation process influence on sample iridescence

The iridescent aspect of this sample was imaged prior and after the electric field treatment and is reported on **Figure S7**. One can see that the sample iridescence was directional at low electric field before this high electric field treatment; the iridescence vanishes at high electric fields, and is finally restored after the electric field has been interrupted. However, the restored iridescence lost its directionality and both light-from-top and light-from-side geometries produce iridescent colors. Note that the samples produced with this fast annealing treatment are still macroscopically inhomogeneous.

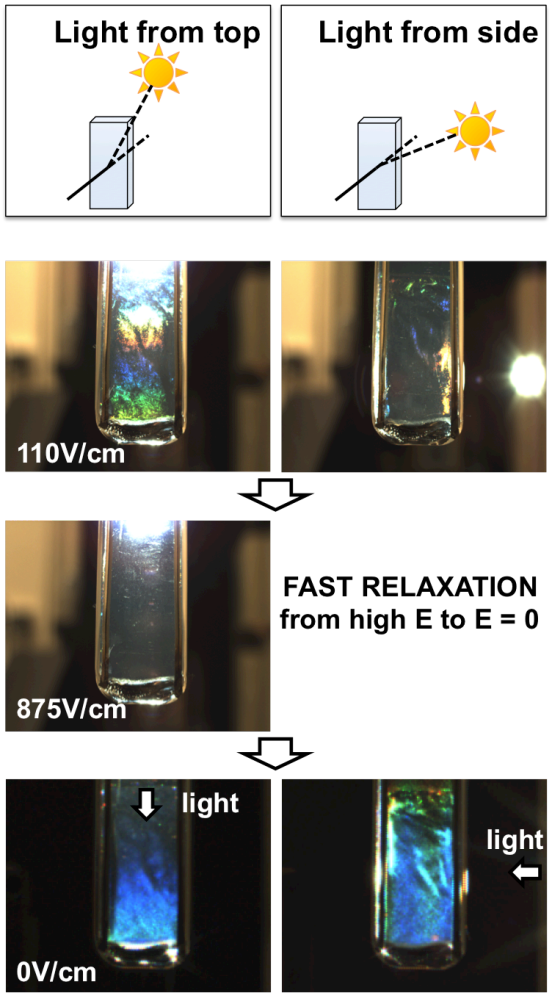

Figure S7. Iridescence of the sample A-1 as observed in two incident light configurations: either aligned (top) or perpendicular (side) with the initial cholesteric axis ***h***. This is compared

(a) prior, (b) during and (c) after application of a strong electric field in an ON-OFF cycle, i.e., where the electric field is applied above the E_c threshold, and quickly suppressed (abrupt field removal). One can see that the initially oriented cholesteric sample (iridescence observable only with light from top) turns transparent when a strong field is applied, and its iridescence is restored when the field is suddenly removed. The iridescence is visible in both light configurations, indicating a randomized orientation of the cholesteric domains.

F.3. Additional notes concerning the figures S6-S7

Cholesterics can be considered as one-dimensional Bragg crystals, i.e. the diffraction occurs only along the vectorial direction $\boldsymbol{k_d}$ contained in the plane defined by the incident light beam $\boldsymbol{k_i}$ and the helix axis $\boldsymbol{h}$ of the diffracting cholesteric domain. At thermodynamics equilibrium, the pitch p in the suspension is fixed but the orientation of the domains is not, and leads to polydomain samples of randomized domain orientation: this explains why the diffraction pattern produces diffraction peaks that merge as a ring of defined diameter (related to the uniform pitch) but undefined angle (leading to a diffraction ring). The same is true for the iridescent observation: if a light source is placed in a specific corner of the background of the sample, the incident light angle theta will define the observed iridescent color, while its azimutal angle ψ will only select the orientation of the domains that contributes to the observed diffraction.

The initially aligned sample (Figure S7, 110 V/cm) contains mostly oriented domains, and as a result appears iridescent only when the domain helix axes $\boldsymbol{h}$ are within the plane defined by the incident light beam $\boldsymbol{k_i}$ and the iridescence viewing direction $\boldsymbol{k_d}$. When a strong field is applied (Figure S7, 875 V/cm), the cholesteric is unwound and no iridescence is observed. After the sudden field removal (fast relaxation treatment), the cholesteric suddenly rewinds into many small cholesteric domains of randomized orientation and the resulting iridescence

can then be observed regardless of the azimutal angle ψ of the incident light (Figure S7, 0 V/cm).

G. Sample relaxation under of electric field slow annealing

The sample relaxation under electric field slow annealing was monitored with laser diffraction, as shown on **Figure S8** from sample C-7.

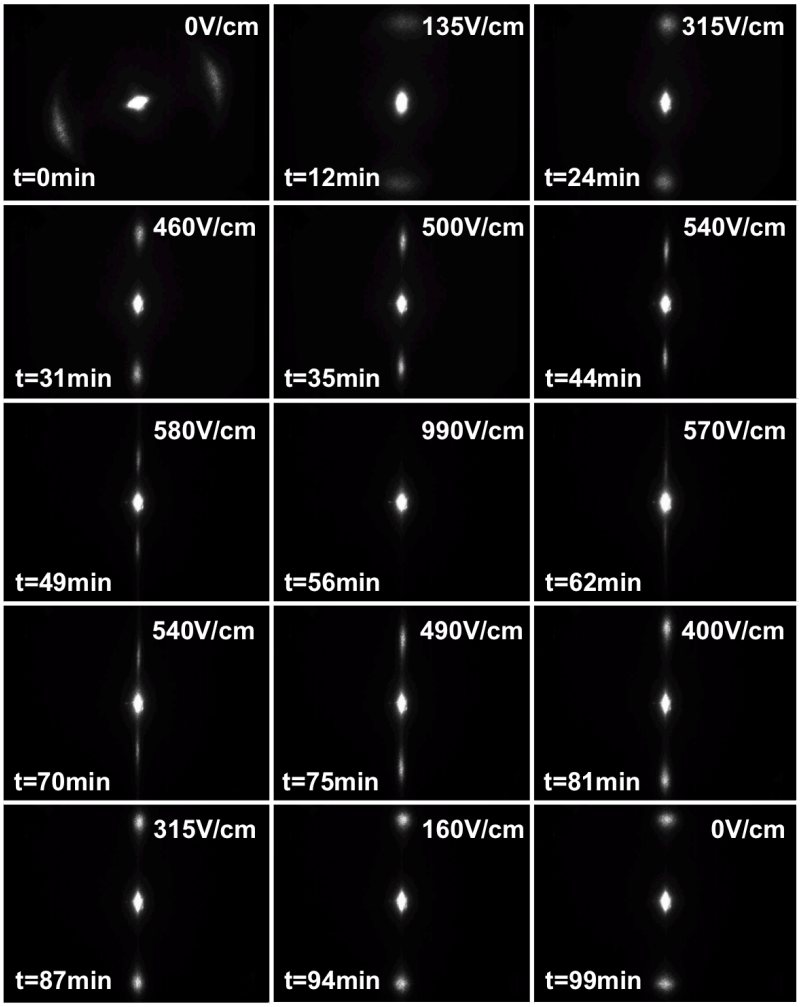

Figure S8. Laser diffraction pattern sequence monitoring the evolution of the cholesteric structure as the field is progressively increased and decreased: starting from an initially disoriented cholesteric sample, the diffraction pattern indicates alignment of the cholesteric, then pitch increase until complete cholesteric unwinding when the field is maximum, followed by the winding of the cholesteric back to its original value, but maintaining the cholesteric orientation even when the field is fully removed.

The complete melting of the cholesteric structure is quickly obtained at fields about ~50% higher than the critical field E_c, and after slow field annealing, the pitch evolution is reproducible and shows little hysteresis (see **Figure S9** on sample C-3).

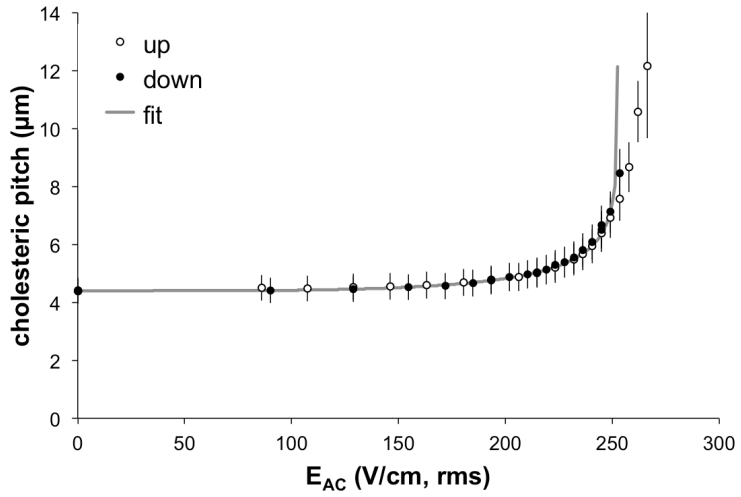

Figure S9. Measure of the cholesteric pitch hysteresis curve under the first electric field exposition ("up") and slowly back to zero ("down"), showing good agreement with the corresponding fit. On the raw data used to derive the curve "up", the diffraction peaks become very broad and poorly defined above the critical field E_c until complete peak disappearance. The pitch under field increase and decrease displayed little hysteresis for $E < E_c$ and the "down" curve was used to fit the model to the data.

H. Transmission Electron Microscopy (TEM) of the individual CNCs used

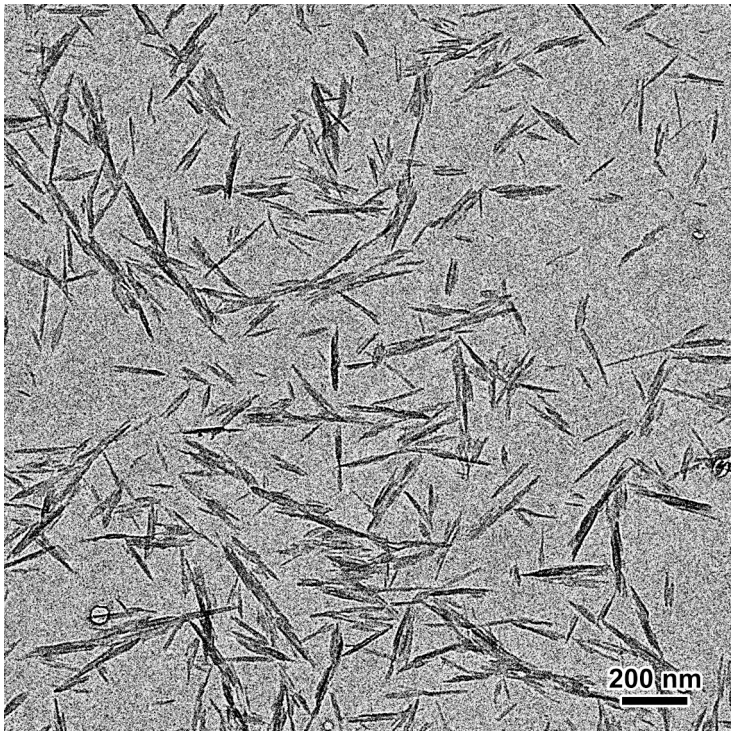

Figure S10. Transmission Electron Microscopy of a CNC suspension. The CNCs were imaged from the aqueous suspension, prior to their transfer into the apolar solvent, as described in the experimental section.

I. References

[1] B. Frka-Petesic, B. Jean, L. Heux, *EPL* **2014**, *107*, 28006.

[2] F. J. Kahn, *Phys. Rev. Lett.* **1970**, *24*, 209.

[3] R. M. Parker, B. Frka-Petesic, G. Guidetti, G. Kamita, G. Consani, C. Abell, S. Vignolini, *ACS Nano* **2016**, *10*, 8443.

[4] Z. Dogic, S. Fraden, *Langmuir* **2000**, *16*, 7820.